TURBULENCE CHARACTERISTICS OF SEMICONFINED IMPINGING ARRAYS OF JETS

Bertrand P. E. Dano
Department of Mechanical Engineering,
Oregon State University, Corvallis, OR 97331, USA
dano@engr.orst.edu

James A. Liburdy
Department of Mechanical Engineering,
Oregon State University, Corvallis, OR 97331, USA
liburdy@engr.orst.edu

ABSTRACT
The crossflow interaction of multiple air jets impinging on a flat surface enclosed by three walls is investigated. Details of the mean and some turbulence quantities for two 7x7 jet arrays are presented: circular and cusped ellipse shape. The Reynolds number ranges from 8,500 to 15,900. Surface flow visualization and PIV measurements of the entire flow field are used to interpret the complex flow characteristics

INTRODUCTION
Many applications use jet impingement to achieve improved cooling of engineering systems. The use of impinging jets in industrial and electronic applications evolved rapidly from a single jet to arrays of jets, thereby providing more uniform cooling. Before 1992, all jet array flow studies have been presented essentially in the absence of a crossflow. Using laser-Doppler velocimetry, Barata (1992) showed that the flow pattern for each jet is similar to a single impinging jet but gives rise to a fountain upwash flow, interacting with the crossflow. Later, Barata (1996) highlighted the presence of a complex three-dimensional "scarf" vortex around each impinging jet. Most recently, Bernard, Brizzi and Bousgarbies (1999) improved these results. Using a combination of flow visualization and laser-Doppler velocity measurement, they proposed a topology of the flow structure including a ground vortex structure and describing the fluid behavior in the vicinity of the plane wall.

Another factor, which may affect the resultant jet array flow field, is the jet orifice geometry. Owens and Liburdy (1995) demonstrated that using an elliptic jet at low Reynolds number improves heat transfer up to 37.5% over a circular jet. But, the mechanism of this improvement is still not clear.

The objective of this paper is to give a better understanding of the turbulent structure of (7x7) jet arrays with crossflow, with different jet orifice geometries: circular and cusped ellipse. The orifice plate and jet geometries are shown in Figure 1. Both shapes have been designed to have the same orifice area: A= 1.267×10^{-6} m^2. The sensitivity to different parameters such as the impingement distance, H/D_H=2 to 4 , the Reynolds number, Re=8,500 to 15,900, and cusped ellipse nozzle orientation are investigated. The long axis of the cusped ellipse being aligned with the crossflow is noted as 0° and the long axis normal to the crossflow is noted as 90° as shown is Figure 1.

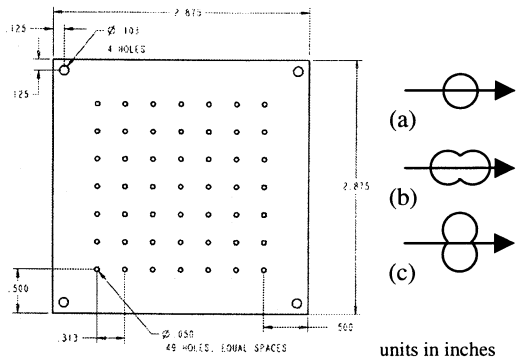

Figure 1. Jet arrays geometry. (a) Circular jet, (b) Cusped Ellipse 0°, (c) Cusped Ellipse 90°

EXPERIMENTAL METHOD
The jet array geometry and the jet configurations are shown in Figure 1. The test facility consists of a stainless steel cubic plenum chamber (30 cm side length) with the orifice plate fastened at the bottom of the chamber and the impingement surface, fastened right below the jet array. A dry-air compressor supplied air to the plenum chamber in which a diffuser plate was installed, breaking down the large scale turbulence of the incoming air and providing a volume of high pressure and low velocity air, right above the orifice plate. The impingement surface had three Plexiglas walls, which together with the impingement surface formed a channel. The jet flow impinged on the bottom plate and escaped out the open side, creating a crossflow. The impingement distance was variable and was

adjusted by placing a calibrated separator between the jet array and the impingement plate.

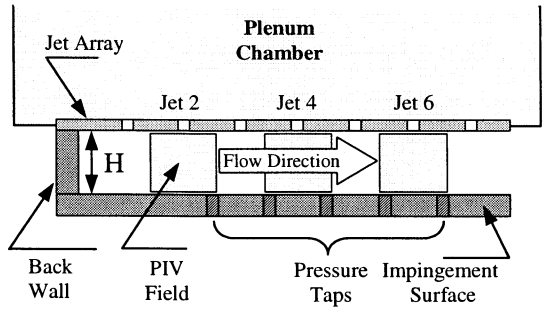

Figure 2: Impingement plate setup and jet locations.

The downstream location along the flow was defined as the crossflow-to-jet velocity ratio, $V_r=V_c/V_j$. It is assumed that the total mass flow rate is evenly divided among the 49 jets and that the increase in crossflow velocity is due only to the upstream jets along the same given row along the downstream direction. V_c is defined as the average velocity of the air flowing through the area formed by the top and bottom of the channel and the space between two rows. V_j is the exit velocity of the jet. As can be seen in Figure 3, V_r is a linear function of the jet position with a smaller slope for larger impingement distance H/D_H.

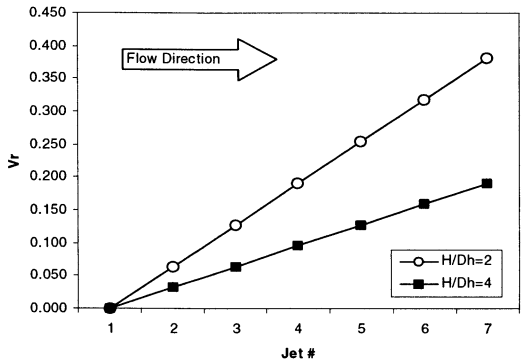

Figure 3: Crossflow-to-jet velocity ratio, V_r versus jet number, measured from the most upstream jet.

The general pattern of the impingement surface was obtained by seeding the flow with TiO_2. The deposit of these 2 to 3 micron-size particles at the stagnation points and slow flowing areas provides a localization of the mean streamlines flow pattern that were recorded and analyzed.

Particle Image Velocimetry (PIV) was performed using a double pulse Nd:YAG laser implemented with an optic system giving a thin laser sheet (1mm thick). The laser sheet was aligned with a designated row of jets along the crossflow direction. The flow was seeded with TiO_2 particles. A digital camera was positioned perpendicular to the laser sheet, looking through one transparent sidewall. Pairs of high-resolution pictures were recorded (1300x1030 pixels) with 2μs time separations. Cross-correlation analysis was used to obtain the instantaneous velocity field of the flow. Over fifty instantaneous velocity flow fields were obtained for each jet and averaged to highlight the mean flow structure and turbulence properties.

From the velocity flow-field, three properties are presented: the vorticity field which was obtained using a centered finite difference scheme, and the turbulent kinetic energy and the mean squared vorticity which were obtained by statistical methods on the velocity fields and vorticity fields data, respectively. The list of PIV tests and the corresponding Reynolds number for each geometry are shown in Table 1.

Jet Array	Jet Number	H/D_H	Re
Circular Jet	2, 4, 6	2,4	9,740 - 15,800
Cusped Ellipse 0°	2, 4, 6	4	8,570 - 13,500
Cusped Ellipse 90°	2, 4, 6	4	8,570 - 13,500

Table 1: PIV tests and conditions

RESULTS

The surface flow visualization provides a good overview of the flow pattern at the impingement surface. As the jets spread over the surface, they create an array of cells defined by four detachment-reattachment zones with a characteristic "horseshoe" shape around each jet. An example is shown in Figure 4. The upstream part is identified as the stagnation zone created by the crossflow and the jet-flow directed upstream. The bands on each side are due to the roll-up of two adjacent jets creating a channelized flow between the jets. Along the lateral direction, the results show a quasi-periodic aspect proving that each row can be considered a partial symmetry plane. Moving downstream from the back to the exit, the crossflow ratio increases and it can be observed that the "horseshoe" shapes of the cells become increasingly more oblong in shape. For jets closer to the back wall, the impingement point is located at the center of the cell. With increasing V_r, the boundaries shift progressively in the downstream direction until the impingement point meets the upstream detachment zone. Similar results can be found for all the different jet array configurations.

The mean velocity flow fields provide significant information on the flow structure. The jet appears to split into a downstream flow and a return-flow. This return flow and the flow coming from the upstream jets create a large recirculation region, a surface vortex that can be observed upstream of the jet column. The downstream flow progressively turns along the sides of the jets into a parallel flow along the impingement surface. Moving downstream from jet 2 to jet 6, the surface vortex size decrease from

the entire height of the channel to only half of the height while the angular velocity increase. Its center of rotation gets closer to the jet column and stays close to the impingement surface. In Figure 5, the mean velocity flow field, based on the PIV data is shown in the proximity of the impingement surface for the circular jet for jet 6. One can see how the surface vortex is just upstream of the jet column. The gap between the impingement surface and the first row of vectors is due to the PIV analysis overlap method and corresponds to ½ of the interrogation cell size.

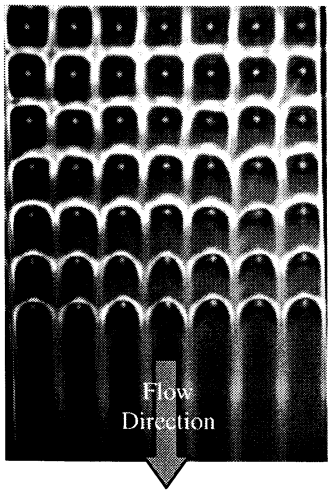

Figure 4: Surface flow pattern for circular jet, H/D_H=4, Re=10,000.

The mean vorticity fields were obtained using a cell-centered finite difference scheme based on the instantaneous velocity field, and then the fields were averaged together. These results provide details of the various vortex locations resulting from the interaction of the crossflow and the jets. Pairs of counter-rotating vorticity are visible, delimiting the jet shearing layers. However, results are not symmetric on the upstream and the downstream side of the jet column. Results are shown in Figure 6a for H/D_H=4, Re=9,790. For lower Re, the jet is well defined. For increasing Re, the symmetry is lost and pockets of vorticity can be found distributed over the channel. In Figure 6a, the symmetry lack of symmetry can be observed for the circular jet at the jet 6 location. The shearing of the jet column is reinforced upstream by the surface vortex and the increase of vorticity downstream of the impingement point.

The turbulent kinetic energy fields and mean squared vorticity fields were obtained by using statistical methods on the instantaneous velocity fields and vorticity fields data, respectively. Figure 6b and 6c show these results for the circular jet at the jet 6 location. The turbulent kinetic energy is mainly located in the jet column and at the impingement

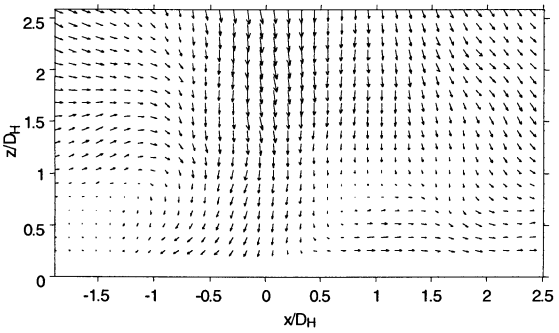

Figure 5: Circular jet. Mean velocity flow field, H/D_H=4, Jet 6, V_r =0.159, Re=9,790.

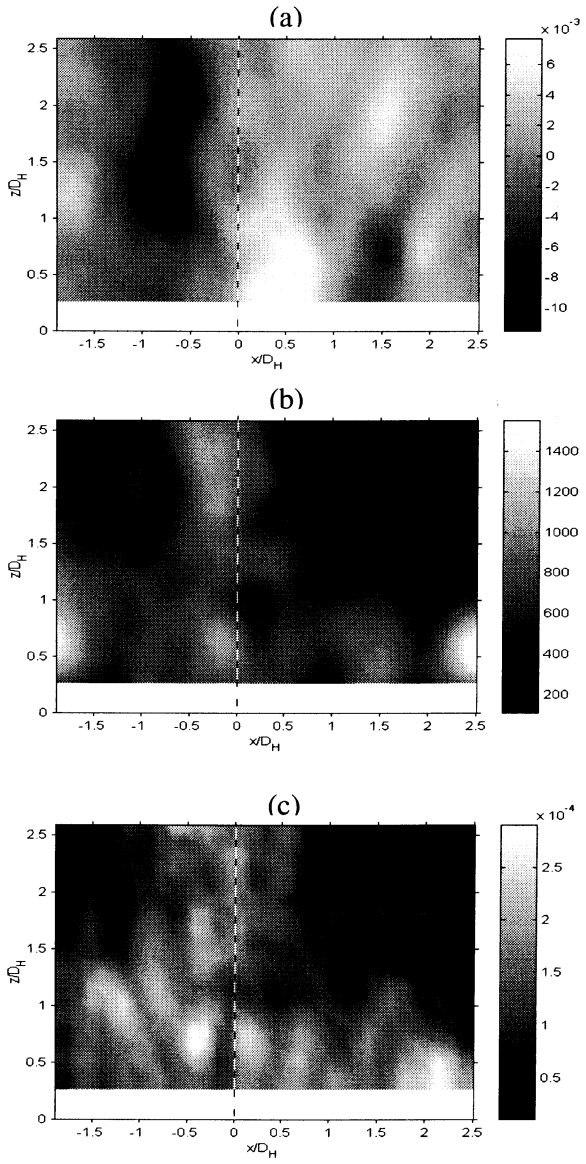

Figure 6: Circular jet, H/D_H=4, Jet 6, V_r =0.159, Re=9,790. (a) Mean vorticity, (b) Turbulent kinetic energy, (c) Mean squared vorticity.

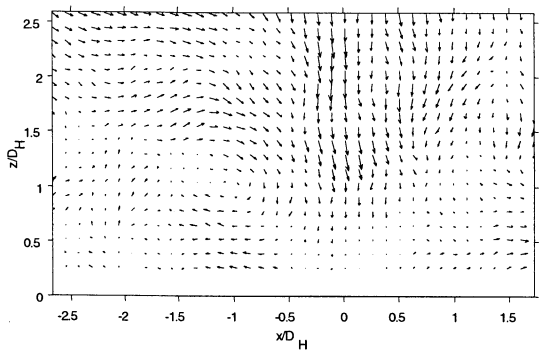

Figure 7: Cusped ellipse 0° jet. Mean velocity flow field, H/D_H=4, Jet 6, V_r =0.159, Re=8,500.

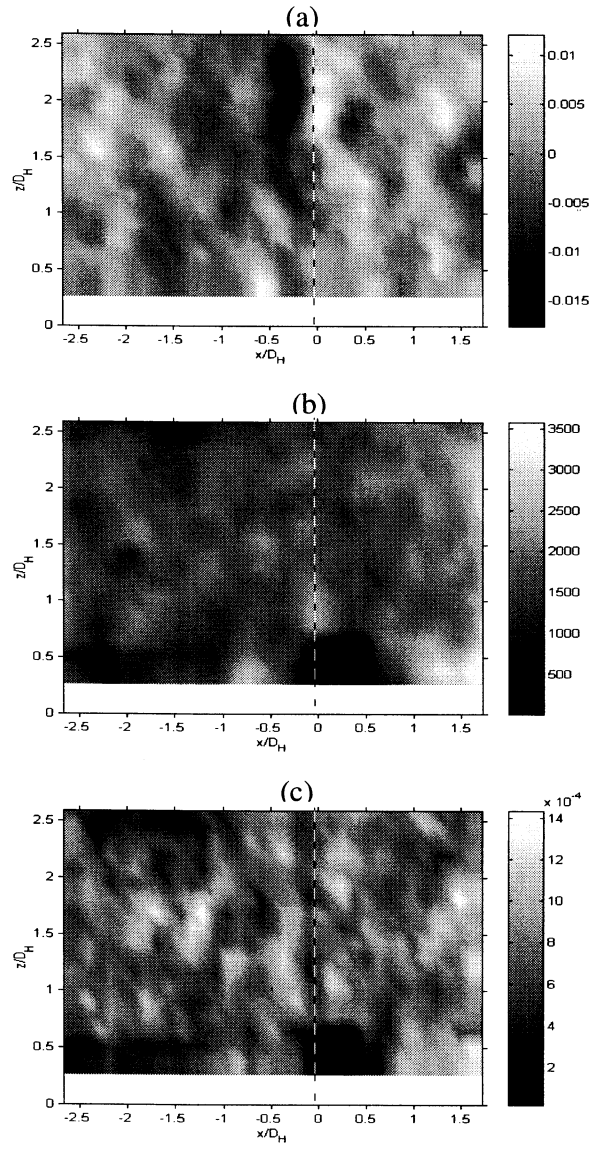

Figure 8: Cusped ellipse 0° jet. H/D_H=4, Jet 6, V_r =0.159, Re=8,500. (a) Mean vorticity, (b) Turbulent kinetic Energy, (c) Mean squared vorticity.

surface. Using the mean squared vorticity as a measure of turbulent dissipation rate, Figure 6c illustrates how the dissipation is also concentrated in the jet column and near the impingement surface. But it be noted that it is not uniform, but rather intermittent in its distribution.

The circular jet and the cusped ellipse (0°) appear to have very comparable flow structures. In Figure 7, a similar surface vortex is observed for the same conditions as the circular jet (same mass flow rate). For most of the configurations, a surface vortex is observed upstream of the jet column and the jet column appears well defined. Meanwhile, the flow appears more diffuse for the cusped ellipse jet, even at low Re, as can be seen in Figure 8a. The turbulent kinetic energy and mean squared vorticity fields show greater spreading and a more intermittent distribution appears to exist, as depicted in Figures 8b and 8c.

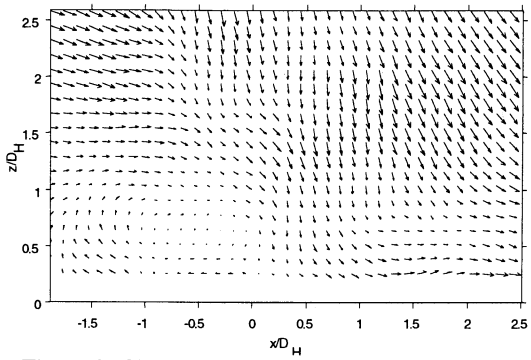

Figure 9: Circular jet. Mean velocity flow field, H/D_H=4, Jet 6, V_r =0.159, Re=15,800.

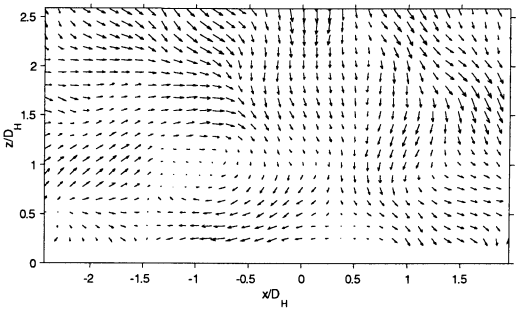

Figure 10: Cusped ellipse 0° jet. Mean velocity flow field, H/D_H=4, Jet 6, V_r =0.159, Re=13,500.

Similar results are found for higher values of Re. In Figures 9 and 10 are the mean velocity flow fields at the jet 6 location for the same higher mass flow rate for the circular and cusped ellipse (0°) jet, respectively. For the circular jet, the surface vortex seems to collide strongly with the jet column, deflecting the column significantly downstream. The surface vortex size appears to expand in the streamwise direction while it shrinks in height. The jet column velocity reaches a minimum just at the

interface with the surface vortex, before accelerating in the downstream direction. Consequently, the entrainment of the downstream flow is expected to increase. A major change is observed for the cusped ellipse (0°) jet, as shown in Figure 10. As the jet separate into a downstream and return-flow a contraction of the jet column is observed at $1D_H$ above the impingement surface. This appears to create a slight "return-curve" of the downstream flow creating a larger and more diffuse impingement zone. This is speculated to be due to the axis switching effect, typical for non-axisymmetric jets where the major and minor axis interchange some distance downstream from the jet exit. This would also explain the observed reduction of the jet column velocity, resulting from flow transfer in the transversal direction.

The mean flow pattern for the cusped ellipse (90°) is radically different than the other two, as shown in Figure 11. No surface vortex is observed in the mean velocity flow field except close to the back wall where a large and weak recirculation structure is observed. Meanwhile, inspection of some of the instantaneous velocity flow fields reveal the existence of a surface vortex. Therefore, this vortex must be periodically destroyed by the strong crossflow.

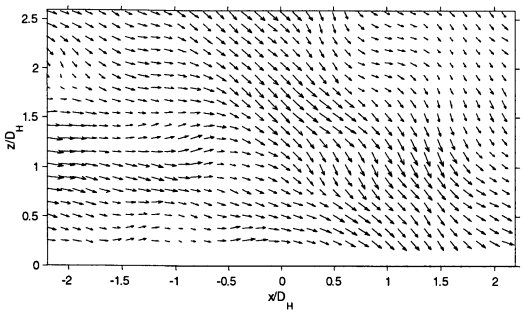

Figure 11: Cusped ellipse 90° jet. Mean velocity flow field, H/D_H=4, Jet 6, V_r =0.159, Re=13,500.

In order to compare the flow characteristics for each jet geometry, spatially averaged levels of vorticity, turbulent kinetic energy and mean squared vorticity were determined. Values were averaged in the section of the flow corresponding to the impinging area defined as: $-1.5 < X/D_H < 1.5$ and $0 < Z/D_H < 2.5$ measured about the impingement point and then averaged over three jets along the downstream position: jets 2, 4 and 6. The mean vorticity level, $\overline{W^2}$, was computed based on the squared values of the mean vorticity to account for positive and negative values. Table 2 shows the different jet array configuration with the corresponding Re.

Figure 12b shows the spatially averaged levels of $\overline{tke}$ for each jet array. One can clearly see that the cusped ellipse in the (0°) position generates more turbulence than in the (90°) position for both values of Re.

	Reynolds Number	
Jet Array Configuration	Low Re1	High Re2
Circular jet	9,740	15,800
Cusped ellipse (0°)	8,570	13,500
Cusped ellipse (90°)	8,570	13,500

Table 2. Jet array flow conditions for spatial average flow characteristics

Shown in Figure 12a are the overall averaged mean vorticity squared, $\overline{W^2}$ for the various jet geometries and for low Reynolds number (Re1). The "cusped" ellipse shows a much larger spreading of these pockets over the channel associated with a greater level of intensity. Compared to the circular jet, a 16% increase in averaged vorticity, $\overline{W^2}$, is observed for the cusped ellipse (0°) jet array. In the (90°) orientation, the $\overline{W^2}$ level is 4 times smaller. Therefore, significant changes to the mean vorticity level can be made by changes in the jet orifice geometry.

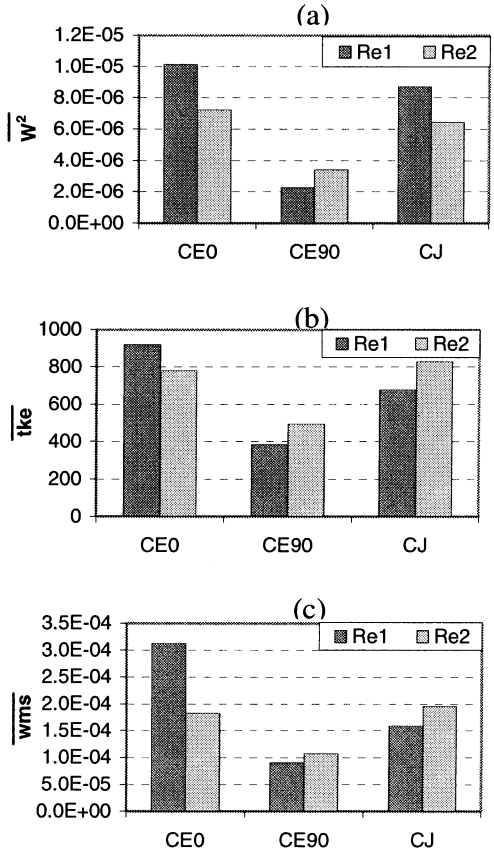

Figure 12: Spatial average flow characteristics. (a) Vorticity, (b) Turbulent kinetic energy, (c) Mean squared vorticity

For the circular jet, a 36% increase in $\overline{tke}$ is observed throughout the overall channel for the lower Re. The mean squared vorticity, $\overline{wms}$ levels show wide variations between th different jet arrays as shown in Figure 11c. Again, one can see that cusped ellipse (0°) generates 97% more "dissipation" than the circular jet while the (90°) configuration has even lower values. For the higher Re, Re2, results are similar.

However, the circular jet and the cusped ellipse in the (0°) configuration have similar intensities in $\overline{tke}$ and the "dissipation" with the circular jet results is essentially the same as the cusped ellipse (0°) jet array. The cusped ellipse (90°) jet array results stay significantly below the values for the two other configurations.

CONCLUSIONS

Surface flow visualization and PIV measurements of the entire flow field were used to interpret the complex flow features of an impinging jet array with crossflow and different jet orifices geometries. The flow visualization of the impinging patterns shows similar results for the different jet orifices geometries. The jets generate cells that progressively expand in size with increasing crossflow. PIV measurements of the entire flow field in the vicinity of the jet exits reveals complex flow structures: a large vortex created by the merging of the crossflow and the jet column return-flow moves towards the jet column as the crossflow increases in strength. This proximity generates multiple turbulent flow patterns. For lower Re, the cusped ellipse jet array placed in the (0°) position, the major axis aligned parallel to the crossflow, appears to generate significantly more turbulence than the circular jet array, while for higher Re, both configurations show similar results. However, for the cusped ellipse in the (90°) position, the major axis normal to the crossflow, the results show significantly smaller levels of turbulence when compared with the circular jets. Meanwhile, evidence of axis switching in the jet column development indicates that a transport in the lateral direction could be a secondary factor to take into account for surface cooling efficiency. This may have consequences for improved surface cooling applications in engineering systems.

REFERENCES

Barata, J.M.M., Durao, D.F.G. and Heitor, M.V., 1992, "Velocity Characteristics of Multiple Impinging Jets Through a Crossflow", *Journal of Fluids Engineering*, Vol. 114, pp. 231-239.

Barata, J.M.M., 1996, "Fountain Flows Produced by Multiple Impinging Jets in a Crossflow", *AIAA Journal*, Vol. 34, No. 12, pp. 2523-2530.

Bernard, A., Brizzi, L.-E. and Bousgarbies, J.-L., 1999, "Study of Several Jets Impinging on a Plane Wall: Visualizations and Laser Velocimetry Investigation", *Transactions of the ASME*, Vol. 121, pp. 808-812.

Owens, R. and Liburdy, J.A., 1995, "Effect of Nozzle Geometry on the Heat Transfer Distribution in a Jet Array," ASME National Heat Transfer Conference.